Journal of King Saud University – Science 32 (2020) 2826–2830

Contents lists available at ScienceDirect

Journal of King Saud University – Science

journal homepage: www.sciencedirect.com

Original article

Synthesis and characterization cobalt phosphate embedded with N doped carbon for water splitting ORR and OER

Tansir Ahamad *, Mu Naushad, Rashed Hassan Mousa, Naif Khalaf, Saad M Alshehri

Department of Chemistry, College of Science, King Saud University, Riyadh 11451, Saudi Arabia

ARTICLE INFO

Article history:
Received 23 February 2020
Revised 6 July 2020
Accepted 8 July 2020
Available online 11 July 2020

Keywords:
Nanoparticles
Carbon materials
Water splitting
$Co_3(PO_4)_2$
Nanocomposite

ABSTRACT

In this study, we have fabricated the $Co_3(PO_4)_2$ nanoparticles and $Co_3(PO_4)_2$-NC doped in N doped carbon nanocomposite. The fabricated nanocomposite was characterized successfully using several analytical techniques. The fabricated nanocomposite was used as electrocatalyst for water splitting, the oxygen evolution reaction (OER) and oxygen reduction reaction (ORR) in 1.0 M KOH solution. The fabricated nanocomposite shows highly porous nature with high surface area about to 372.32 m^2/g. The catalytic results show, the lower limiting overpotential during the ORR (η_{lim} = 0.33 V) and more positive half-wave potential activity than that of commercial platinum on carbon (Pt/C) catalyst. Moreover, the $Co_3(PO_4)_2$-NC exhibit excellent catalytic activity toward OER, with an overpotential of 350 mV at 10 $mAcm^2$ in 1.0 M KOH solution and a relatively low Tafel slope of 60.7 mV dec. In addition, the fabricated catalyst possesses excellent reusability, long term stability with fast electron transfer during the catalytic reactions. These outcomes revealed that the fabricated nanocomposites can be used as low-cost, efficient catalyst for water splitting ORR and OER in metal-air batteries and fuel cells.

1. Introduction

With the increasing of the global energy problems and the increasingly serious environmental pollution, the utilization of photo and electro catalytic technology to get hydrogen has attracted extensive attention; due to hydrogen energy is considered to be one of the most favorable options to fossil fuels (Ashok et al., 2019; Béjar et al., 2019; Chakrabarty et al., 2019). Water splitting is deeming as one of the most favorable strategy for hydrogen production (Chen et al., 2020; Cheng et al., 2020; Deng et al., 2019). Water splitting include, oxygen reduction (ORR, $O_2 + H_2O + 4e^- \rightarrow 4OH^-$) and oxygen evolution (OER, $4OH^- \rightarrow O_2 + 2H_2O + 4e^-$) reactions, which plays a paramount role in energy conversion and storage devices, including metal air-batteries and fuel cells (Fang et al., 2018; Giacco et al., 2018). The greatest challenge for water splitting is to fabricate an efficient catalyst for both the ORR and OER (Li et al., 2020b; Zhang et al., 2019; Zheng et al., 2019; Zhu et al., 2018). Currently, several precious metals including Pt, Ir and Ru based catalyst have been used for water splitting (Ding et al., 2019; Fang et al., 2019; Filimonenkov et al., 2019). The use of these metal based catalysts still limited due their high cost and rear source. Moreover, using of the different catalysts for each side reaction also increase the processing costs and time. Therefore, it is the great demand to developed low coast highly stable bi-functional catalyst (Ishizaki et al., 2020; Jung et al., 2015; Li et al., 2020a). Recently several novel materials, such as metal oxides, carbides, nitrides, sulfides and carbonaceous materials, have been used a catalyst for water splitting (Li et al., 2018; Liu et al., 2017; Lv et al., 2019; Mamtani et al., 2018). Among these materials, metal phosphate especially cobalt phosphate has been used for electrocatalyst for water splitting (Yuan et al., 2016). Moreover, the nanocomposites of hetroatoms doped carbon with these metal phosphates and oxide increased the electrical conductivity as well as the stability of the catalyst in both the acidic and basic condition. Based on these study, herein we have in-situ fabricate $Co_3(PO_4)_2$ nanoparticles in to N doped carbon matrix. The fabricated $Co_3(PO_4)_2$-NC nanocomposite was analyzed using several techniques such as FTIR, TGA, XRD, Raman, SEM, TEM, BET and XPS. As-fabricated $Co_3(PO_4)_2$-NSC nanocomposite has been used for water splitting ORR and OER in 1.0 M KOH solution. The fabricated catalyst shows excellent catalytic efficiency for both OER and ORR as well as excellent reusability, long term stability with fast

* Corresponding author.
E-mail address: tahamed@ksu.edu.sa (T. Ahamad).
Peer review under responsibility of King Saud University.

Production and hosting by Elsevier

https://doi.org/10.1016/j.jksus.2020.07.004
1018-3647/

electron transfer during the catalytic reactions. These outcomes revealed that the fabricated nanocomposites can be used as low-cost, efficient catalyst for water splitting ORR and OER in metal-air batteries and fuel cells.

2. Experimental

2.1. Materials

Cobalt(II) chloride and acetic acid was purchased from Merck, (India). Chitosan, Pt/C and Ru_2O as reference electro-catalysts and other chemicals were purchased Sigma-Aldrich and directly used without further purification. Milli-Q water was used throughout all experiments.

2.2. Fabricate of $Co_3(PO_4)_2$-NC nanocomposite

3.0 g of chitosan was dissolved in deionized water using acetic acid (20 mL aqueous solution) and mixed with 1.25 g of $CoCl_2$was added to this solution and resulting mixture was stirred at room temperature to get the homogenous mixture and then add 0.75 g of $(NH_4)_3PO_4$and then mixed it for another 30 min. The resulting mixture was transferred into steeliness steel autoclave and heat at 250 °C for 24 h. As-resulted hydrochar was further heat treated up to 800 °C, under the follow of argon with a heating rate was 5 °C/min to get $Co_3(PO_4)_2$nanoparticles embedded into N doped carbon ($Co_3(PO_4)_2$-NC).

3. Results and discussion

$Co_3(PO_4)_2$ nanoparticles embedded into N doped carbon [$Co_3(PO_4)_2$-NC] was fabricated using hydrothermal and post-pyrolysis method as illustrated in Fig. 1. The FTIR spectra of the nanocomposite as shown in Fig. 2, show several adsorption peaks at 3416–3234, 2945–2862, 1624, 1534, 1456 and 1392 cm^{-1} assigned to the O–H/N–H, C–H, C═N, C═C, C–O and C–N respectively (Ahamad et al., 2020b; Ahamad et al., 2020c; Ahamad et al., 2019; Al-Kahtani et al., 2018; Naushad et al., 2019). Another peaks at 1053 and 568 cm^{-1}corresponds to P-O and Co-O stretching respectively. The X-ray diffraction (XRD) as illustrated in Fig. 1(a), show diffraction peaks at 2θ = 20.8, 25.84, 31.8, 38.02 43.8, 51.01, and 55.47° and assigned to (011), (210), (220), (031), (−122), (−132), and (312) planes respectively for $Co_3(PO_4)_2$ (JCPDS No.01–0373) (Liu et al., 2018; Shi et al., 2020). Another broad diffraction peak at 2θ = 26.0°, suggest the formation of graphitic structure in the nanocomposite. The presence of the graphite carbon in the nanocomposite and doping of the N was further supported using Raman spectra. The nanocomposite shows two peaks Raman peaks at 1346 and 1583 cm^{-1}assinged to the G and D band respectively. Another peaks at low frequency at 971 cm^{-1} support the formation of $(PO_4)^{3-}$ into the carbon matrix. The porosity of the nanocomposite was determine using the N_2 adsorption and desorption isotherm and the BET surface area was found to be 372.32 m^2/g, Moreover the pore size distribution was calculated from desorption data using the BJH model and was found in the range of 4–5 nm as shown in Fig. 1(c).

The morphology and structure of the as-fabricated $Co_3(PO_4)_2$-NC was determine by scanning electron microscopy (SEM). As shown in Fig. 1(d), The SEM images show the spherical $Co_3(PO_4)_2$nanoparticles were embedded uniformly into the carbon matrix. Fig. 1(e) display the details of the nanocomposites and show that $Co_3(PO_4)_2$-NC is composed of a large amount of $Co_3(PO_4)_2$ nanoparticles with the range of 24–26 nm and dispersed on the surface or into the carbon matrix. The strong interaction between the $Co_3(PO_4)_2$ nanoparticles and the $Co_3(PO_4)_2$-NC, enhancing the overall electron transfer capability. The high resolution TEM images as shown in Fig. 3(f), show the crystalline nature of the $Co_3(PO_4)_2$nanoparticles and the lattice fringes was found to be0.244 nm for (121) plans. The selected area electron diffraction pattern as illustrated in inserted figure display the electron diffraction plane (100), (011) and (01–1) of monoclinic cobalt phosphate (Zhou et al., 2016).The elemental composition and the metal oxidation state of the nanocomposite was determine using XPS, as shown in Fig. 2(a), the nanocomposite shows the presence of C, N, O, Co and P elements. The spectra for C1s is shown in Fig. 2(b) and split four peaks at 283.6, 284.4, 285.3 and 287.42 eV corresponding to the C–C/C = C, C-N/C-O and C = O/C = N and –O–C═O respectively (Ahamad et al., 2020a).

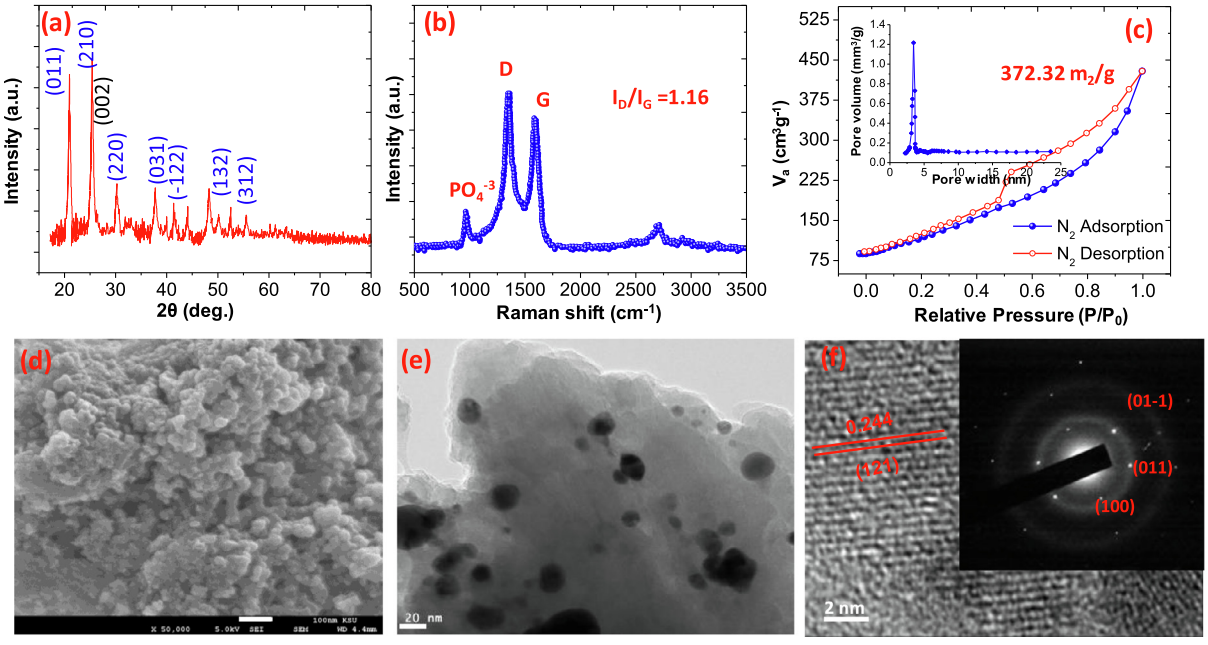

Fig. 1. (a) XRD (b) Raman (c) N_2 adsorption and desorption isotherm (d) SEM (e) TEM and (f) HRTEM and SAED of $Co_3(PO_4)_2$-NC.

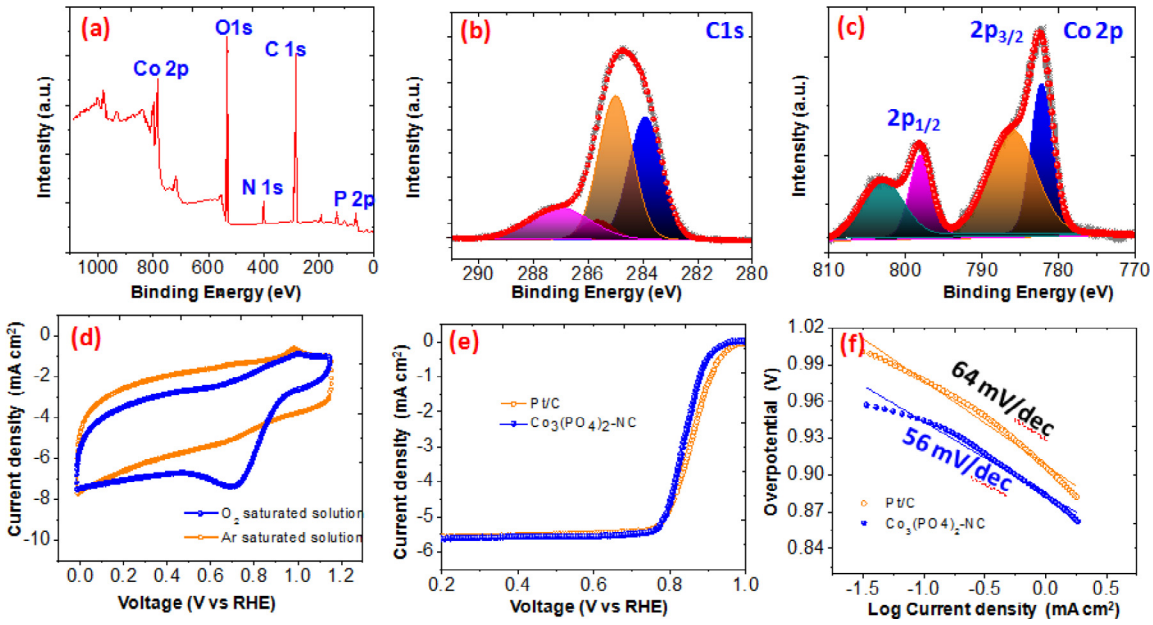

Fig. 2. (a) XPS of $Co_3(PO_4)_2$-NC (b) C1s deconvoluted peaks (c) Co 2p deconvoluted peaks (c) CV (e) LSV and (f) tafel plot for $Co_3(PO_4)_2$-NC in 1.0 M KOH solution.

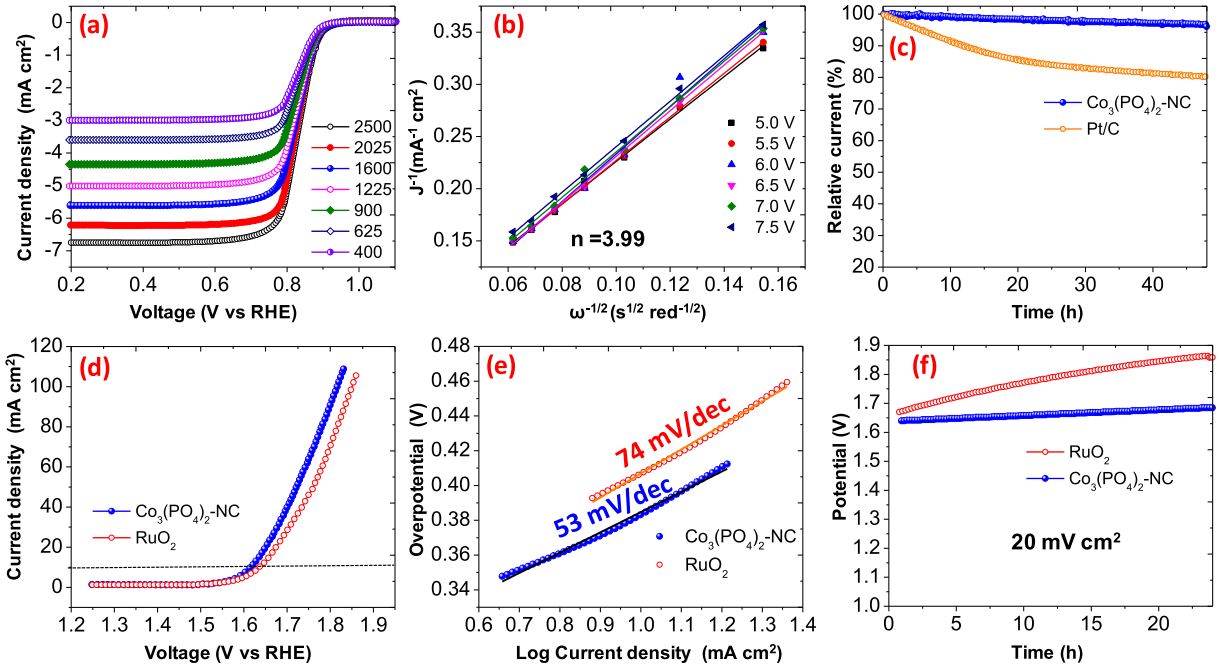

Fig. 3. (a) LSV at different rotation (b) K-L plot (c) chronopotentiometric curves for ORR (d) LSV for OER (e) Tafel plot (d) chronopotentiometric curves for OER.

Fig. 2(c) show the Co 2p deconvoluted into four peaks at 782.21 ($2P_{3/2}$), 786.23, 796.3 ($2P_{1/2}$) and 804.21 eV support the presence of Co^{2+}. The N1s spectra was split into three peaks belongs to the pyridinic N, pyrrolic N, graphitic N and display the peaks at 398.17, 499.23, and 401.05 eV respectively as shown in figure SF-3 (Khalaf et al., 2019). The P 2p region of the sample displayed two peaks at 133.2 eV and 134.4 eV binding energies assigned to the to the 2p3/2 and 2p1/2 core levels of the central phosphorous atoms in the phosphate groups. The O1s shown two peaks at 532.12 and 533.54 eV due to the carbon oxygen and phosphate oxygen bond respectively as shown in supporting figure SF-4.

4. Electro-catalytic activities

The electrons transfer and the electrical conductivity of catalysts were determine using electrochemical impedance spectroscopy (EIS). As shown in supporting figure (SF-5), It was notices that $Co_3(Po)_4$-NC shows the smaller semicircle radius of the Nyquist plots indicate the lower charge transfer resistance and a higher electron and charge transfer efficiency compared to $Co_3(Po)_4$. The electro-catalytic activities of the catalyst for ORR was carried out in 0.1 M KOH, as the CV was presented in the Fig. 2(d), these results revealed that under the O_2 saturated

solution exhibit the ORR peak at 0.834 V, while in the presence of Ar saturated solution this peak was diaper. These results support the fabricated nanocomposite show the ORR behavior in the presence of oxygen. Further the ORR was carried out using linear sweep voltammetry (LSV) with a rotating rate between 400 and 2500 rpm. The LSV curve with a rotating rate of 1600 rpm and is presented in Fig. 2(e), the onset and half wave-potential for $Co_3(PO_4)_2$-NC was found to be 0.964 and 0.831 V. The CV and the LSV results of $Co_3(PO_4)_2$-NC was compared with commercial Pt/C catalyst. To determine the kinetics of the ORR the tafel slope was plotted. As shown in Fig. 2(f) the tafel slop was determine via based on the Fig. 2(e) and the tafel slope for $Co_3(PO_4)_2$-NC was found to be 56 mV/decade, that is smaller than that of Pt/C (64 mV/ decade) and show excellent ORR activities in 0.1 M KOH. As shown in Fig. 3(b), the transfer electron number was calculated using Koutecky–Levich (K–L) plots which were derived from the RED results as shown in Fig. 3(a). the results revealed that the ORR react was carried out about to 4 electron system as shown in supporting information(Yuan et al., 2016). It was reported that an Co atom in $Co_3(PO_4)_2$-NC catalyst structure helps to develop strong back bonding with the adsorbed molecular oxygen, which can cause an increase in O–O bond distance and thus facilitates ORR, based on the molecular orbital theory.(Zhao and Yuan, 2017), In alkaline medium the reaction was proceed via 4 e- way ($O_2 + 2H_2O + 4e^- \rightarrow 4OH^-$) .

To determine the stability of the electrocatalyst the chronoamperometry was carried out and only 3.6% of the current loss was observed after 48 h, while in the case of Pt/C about to 20.2% current loss was noticed in the similar condition. The OER performance of $Co_3(PO_4)_2$-NC nanocomposite was investigated in the O_2 saturated 1.0 M KOH solution and corresponding polarization curve were obtained from LSV. As shown in Fig. 3(d), the LSV plot of the RuO_2 and $Co_3(PO_4)_2$-NC nanocomposite show the over potential 293 mV and 296 mV to get a current density of 10 mA cm^{-2}. The OER kinetics was determine via the tafel plots (53 mV dec^{-1}) derived from polarization curves and the results show that the fabricated nanocomposite show smaller slope then that of RuO_2 (74 mV dec^{-1})(Huang et al., 2019). These outcomes revealed that the $Co_3(PO_4)_2$-NC catalyst show faster OER than commercial catalyst RuO_2. The results showed that the OER reaction is proposed to be assisted by phosphate groups which are directly connected to cobalt and act as proton acceptors. Phosphates can move and shuttle protons freely as the $Co_3(PO_4)_2$-NC catalyst experiences iterative oxidation/reduction cycles which influence the charge transfer. In alkaline medium the reaction proceeds as, $4OH^-_{(aq)} \rightarrow 2H_2O_{(aq)} + 4e^- + O_{2(g)}$ as shown below in equation (1)

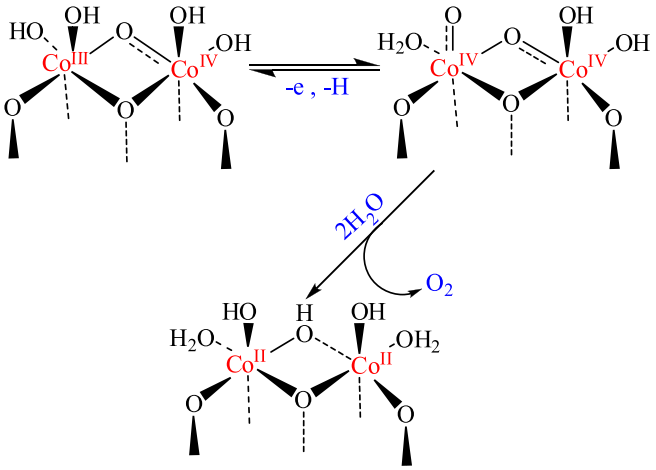

(1)

The chronopotentiometric curves at current density of 20 mA cm^{-2}, was carried out for 24 h and the results revealed that the real-time potential presents slight increase, whereas the RuO_2 catalyst exhibits a continuous increasing the potential during the test.

5. Conclusion

Herein, we have successfully fabricated the $Co_3(PO_4)_2$-NC nanocomposite and used as bifunctional electrocatalyst for ORR and OERin basic medium. As-fabricated $Co_3(PO_4)_2$-NC show excellent catalytic performance for ORR and OER, equivalent to or better than commercial catalyst Pt/C and RuO_2. Due to the easy synthetic process, extensive material availability, and high catalytic activity and stability, the fabricated nanocomposite will also be helpful for other electro catalytic applications.

Declaration of Competing Interest

The authors declare that they have no known competing financial interests or personal relationships that could have appeared to influence the work reported in this paper.

Acknowledgment

The authors extend their sincere appreciation to the Deanship of Scientific Research at King Saud University for funding this work through research group no (RG-1438-026).

Appendix A. Supplementary data

Supplementary data to this article can be found online at https://doi.org/10.1016/j.jksus.2020.07.004.

References

Ahamad, T., Naushad, M., Al-Saeedi, S.I., Alshehri, S.M., 2020a. N/S-doped carbon embedded with AgNPs as a highly efficient catalyst for the reduction of toxic organic pollutants. Mater. Lett. 264, 127310.

Ahamad, T., Naushad, M., Al-Shahrani, T., Al-hokbany, N., Alshehri, S.M., 2020b. Preparation of chitosan based magnetic nanocomposite for tetracycline adsorption: Kinetic and thermodynamic studies. Int. J. Biol. Macromol. 147, 258–267.

Ahamad, T., Naushad, M., Alshheri, S.M., 2020c. Fabrication of highly porous N/S doped carbon embedded with CuO/CuS nanoparticles for NH3 gas sensing. Mater. Lett. 127515

Ahamad, T., Naushad, M., Eldesoky, G.E., Alqadami, A.A., Khan, A., 2019. Synthesis and characterization of egg-albumen-formaldehyde based magnetic polymeric resin (MPR): Highly efficient adsorbent for Cd(II) ion removal from aqueous medium. J. Mol. Liq. 286, 110951.

Al-Kahtani, A.A., Almuqati, T., Alhokbany, N., Ahamad, T., Naushad, M., Alshehri, S. M., 2018. A clean approach for the reduction of hazardous 4-nitrophenol using gold nanoparticles decorated multiwalled carbon nanotubes. J. Cleaner Prod. 191, 429–435.

Ashok, A., Kumar, A., Matin, M.A., Tarlochan, F., 2019. Probing the effect of combustion controlled surface alloying in silver and copper towards ORR and OER in alkaline medium. J. Electroanal. Chem. 844, 66–77.

Béjar, J., Álvarez-Contreras, L., Ledesma-García, J., Arjona, N., Arriaga, L.G., 2019. Electrocatalytic evaluation of Co3O4 and NiCo2O4 rosettes-like hierarchical spinel as bifunctional materials for oxygen evolution (OER) and reduction (ORR) reactions in alkaline media. J. Electroanal. Chem. 847, 113190.

Chakrabarty, S., Mukherjee, A., Su, W.-N., Basu, S., 2019. Improved bi-functional ORR and OER catalytic activity of reduced graphene oxide supported ZnCo2O4 microsphere. Int. J. Hydrogen Energy 44 (3), 1565–1578.

Chen, D., Zhu, J., Mu, X., Cheng, R., Li, W., Liu, S., Pu, Z., Lin, C., Mu, S., 2020. Nitrogen-Doped carbon coupled FeNi3 intermetallic compound as advanced bifunctional electrocatalyst for OER, ORR and zn-air batteries. Appl. Catal. B 268, 118729.

Cheng, W., Yuan, P., Lv, Z., Guo, Y., Qiao, Y., Xue, X., Liu, X., Bai, W., Wang, K., Xu, Q., Zhang, J., 2020. Boosting defective carbon by anchoring well-defined atomically dispersed metal-N4 sites for ORR, OER, and Zn-air batteries. Appl. Catal. B 260, 118198.

Deng, Q., Zhao, J., Wu, T., Chen, G., Hansen, H.A., Vegge, T., 2019. 2D transition metal–TCNQ sheets as bifunctional single-atom catalysts for oxygen reduction and evolution reaction (ORR/OER). J. Catal. 370, 378–384.

Ding, J., Wang, P., Ji, S., Wang, H., Linkov, V., Wang, R., 2019. N-doped mesoporous FeNx/carbon as ORR and OER bifunctional electrocatalyst for rechargeable zinc-air batteries. Electrochim. Acta 296, 653–661.

Fang, H., Huang, T., Sun, Y., Kang, B., Liang, D., Yao, S., Yu, J., Dinesh, M.M., Wu, S., Lee, J.Y., Mao, S., 2019. Metal-organic framework-derived core-shell-structured nitrogen-doped CoCx/FeCo@C hybrid supported by reduced graphene oxide sheets as high performance bifunctional electrocatalysts for ORR and OER. J. Catal. 371, 185–195.

Fang, J., Hu, L., Wang, M., Gan, L., Chen, C., Jiang, Y., Xiao, B., Lai, Y., Li, J., 2018. NiO-Fe2O3/carbon nanotubes composite as bifunctional electrocatalyst for rechargeable Zn-air batteries. Mater. Lett. 218, 36–39.

Filimonenkov, I.S., Bouillet, C., Kéranguéven, G., Simonov, P.A., Tsirlina, G.A., Savinova, E.R., 2019. Carbon materials as additives to the OER catalysts: RRDE study of carbon corrosion at high anodic potentials. Electrochim. Acta 321, 134657.

Giacco, D., Marrani, A.G., Brutti, S., 2018. Enhancement of the performance in Li-O2 cells of a NiCo2O4 based porous positive electrode by Cr(III) doping. Mater. Lett. 224, 113–117.

Huang, Z.-Q., Lu, W.-X., Wang, B., Chen, W.-J., Xie, J.-L., Pan, D.-S., Zhou, L.-L., Song, J.-L., 2019. A mesoporous C, N-co doped Co-based phosphate ultrathin nanosheet derived from a phosphonate-based-MOF as an efficient electrocatalyst for water oxidation. Catal. Sci. Technol. 9 (17), 4718–4724.

Ishizaki, M., Fujii, H., Toshima, K., Tanno, H., Sutoh, H., Kurihara, M., 2020. Preparation of Co-Fe oxides immobilized on carbon paper using water-dispersible Prussian-blue analog nanoparticles and their oxygen evolution reaction (OER) catalytic activities. Inorg. Chim. Acta 502, 119345.

Jung, J., Song, K., Bae, Y., Choi, S.-I., Park, M., Cho, E., Kang, K., Kang, Y.-M., 2015. Achieving outstanding Li+-ORR and -OER activities via edge- and corner-embedded bimetallic nanocubes for rechargeable Li–O2 batteries. Nano Energy 18, 71–80.

Khalaf, N., Ahamad, T., Naushad, M., Al-hokbany, N., Al-Saeedi, S.I., Almotairi, S., Alshehri, S.M., 2019. Chitosan polymer complex derived nanocomposite (AgNPs/NSC) for electrochemical non-enzymatic glucose sensor. International Journal of Biological. Macromolecules.

Li, C., Zhou, E., Yu, Z., Liu, H., Xiong, M., 2020a. Tailor-made open porous 2D CoFe/SN-carbon with slightly weakened adsorption strength of ORR/OER intermediates as remarkable electrocatalysts toward zinc-air batteries. Appl. Catal. B 269, 118771.

Li, J., Liu, G., Liu, B., Min, Z., Qian, D., Jiang, J., Li, J., 2018. An extremely facile route to Co2P encased in N, P-codoped carbon layers: Highly efficient bifunctional electrocatalysts for ORR and OER. Int. J. Hydrogen Energy 43 (3), 1365–1374.

Li, X., Yang, X., Xue, H., Pang, H., Xu, Q., 2020b. Metal–organic frameworks as a platform for clean energy applications. EnergyChem 2, (2) 100027.

Liu, H., Liu, X., Mao, Z., Zhao, Z., Peng, X., Luo, J., Sun, X., 2018. Plasma-activated Co3(PO4)2 nanosheet arrays with Co3+-Rich surfaces for overall water splitting. J. Power Sources 400, 190–197.

Liu, K., Li, J., Wang, Q., Wang, X., Qian, D., Jiang, J., Li, J., Chen, Z., 2017. Designed synthesis of LaCoO3/N-doped reduced graphene oxide nanohybrid as an efficient bifunctional electrocatalyst for ORR and OER in alkaline medium. J. Alloy. Compd. 725, 260–269.

Lv, X., Wei, W., Wang, H., Huang, B., Dai, Y., 2019. Multifunctional electrocatalyst PtM with low Pt loading and high activity towards hydrogen and oxygen electrode reactions: A computational study. Appl. Catal. B 255, 117743.

Mamtani, K., Jain, D., Dogu, D., Gustin, V., Gunduz, S., Co, A.C., Ozkan, U.S., 2018. Insights into oxygen reduction reaction (ORR) and oxygen evolution reaction (OER) active sites for nitrogen-doped carbon nanostructures (CNx) in acidic media. Appl. Catal. B 220, 88–97.

Naushad, M., Ahamad, T., Al-Ghanim, K.A., Al-Muhtaseb, A.a.H., Eldesoky, G.E., Khan, A.A., 2019. A highly porous nanocomposite (Fe3O4@BFR) for the removal of toxic Cd(II) ions from aqueous environment: Adsorption modelling and regeneration study. Composites Part B: Engineering 172, 179-185.

Shi, W., Li, M., Huang, X., Ren, H., Guo, F., Yan, C., 2020. Three-dimensional Z-Scheme Ag3PO4/Co3(PO4)2@Ag heterojunction for improved visible-light photocatalytic degradation activity of tetracycline. J. Alloy. Compd. 818, 152883.

Yuan, C.-Z., Jiang, Y.-F., Wang, Z., Xie, X., Yang, Z.-K., Yousaf, A.B., Xu, A.-W., 2016. Cobalt phosphate nanoparticles decorated with nitrogen-doped carbon layers as highly active and stable electrocatalysts for the oxygen evolution reaction. J. Mater. Chem. A 4 (21), 8155–8160.

Zhang, Y., Liu, J., Li, S.-L., Su, Z.-M., Lan, Y.-Q., 2019. Polyoxometalate-based materials for sustainable and clean energy conversion and storage. EnergyChem 1, (3) 100021.

Zhao, H., Yuan, Z.-Y., 2017. Transition metal–phosphorus-based materials for electrocatalytic energy conversion reactions. Catal. Sci. Technol. 7 (2), 330–347.

Zheng, S., Guo, X., Xue, H., Pan, K., Liu, C., Pang, H., 2019. Facile one-pot generation of metal oxide/hydroxide@metal–organic framework composites: highly efficient bifunctional electrocatalysts for overall water splitting. Chem. Commun. 55 (73), 10904–10907.

Zhou, T., Du, Y., Yin, S., Tian, X., Yang, H., Wang, X., Liu, B., Zheng, H., Qiao, S., Xu, R., 2016. Nitrogen-doped cobalt phosphate@nanocarbon hybrids for efficient electrocatalytic oxygen reduction. Energy Environ. Sci. 9 (8), 2563–2570.

Zhu, R., Ding, J., Xu, Y., Yang, J., Xu, Q., Pang, H., 2018. π-Conjugated Molecule Boosts Metal-Organic Frameworks as Efficient Oxygen Evolution Reaction Catalysts. Small 14 (50), 1803576.